The sliding clamp tethers the endonuclease domain of MutL to DNA

Monica C. Pillon[1], Vignesh M.P. Babu[2,3], Justin R. Randall[5], Jiudou Cai[1],
Lyle A. Simmons[5], Mark D. Sutton[2,3,4], Alba Guarné[1]

The supplementary material contains three tables, eight figures and two movies:

Supplementary Table 1: Concentration-dependency of I0, Rg, and Dmax.

Protein	Concentration (μM)	I0/conc	Rg (Å)**	D_{max} (Å)
eβ	186	0.018	32.3	83
	93	0.019	33.1	90
	47	0.018	32.9	90
eL^{C}	364	0.004	31.3	100
	182	0.004	31.9	100
	91	0.004	31.9	102
eL^{C}-eβ	123	0.029	34.6	100
	61	0.029	35.5	102
	38.5	0.033	35.3	101
	19.5	0.030	36.0	104
	9.5	0.031	35.6	103
bβ	73	0.024*	37.4	104
	44	0.023*	37.1	105
	32	0.016	36.1	100
	27	0.019	36.7	103
bL^{CI}	218	0.003	33.6	112
	165	0.003	33.7	112
	88	0.003	33.1	110
bL^{CI}-bβ	37	0.080	42.1	139
	30	0.080	41.7	140
	22	0.080	41.7	138

* Samples were collected following a filament change resulting in a more intense beam
** Rg determined using the GNOM program from the ATSAS 2.6.0 package

Supplementary Table 2: SAXS data-collection and scattering-derived parameters

	eβ	**eMutL^{CTD}**	**bβ**	**bMutL^{CTDI}**
Data-collection parameters				
Exposure time (min)	60	60	60	120
Concentration (μM)	93	91/364*	32	165
Structural parameters				
I_0 (cm^{-1}) [from Guinier]	1.7 ± 0.0	0.4 ± 0.0	0.5 ± 0.0	0.6 ± 0.0
R_g (Å) [from Guinier]	33.4 ± 0.2	30.8 ± 0.9	37.9 ±0.5	32.1 ± 0.4
I_0 (cm^{-1}) [from P(r)]	1.7 ± 0.0	0.4 ± 0.0	0.5 ± 0.0	0.6 ± 0.0
R_g (Å) [from P(r)]	32.9 ± 0.1	33.0 ± 0.2	36.1 ± 0.1	33.7 ± 0.3
D_{max} (Å)	90	107	100	112
Experimental MW [from Q_R][&]	85,855 Da	43,529 Da	102,663 Da	45,390 Da
Calculated MW	81,263 Da	41,108 Da	90,894 Da	45,500 Da
Ab initio analysis	*DAMMIF/ DAMMIN*	*DAMMIF/ DAMMIN*	*DAMMIN*	*DAMMIF*
χ^2 of *ab initio* models	1.1	1.0-1.1	1.2	0.9
χ^2 (Crysol)	1.3	1.1	1.5	1.0
PDB	1MMI	1X9Z	4RT6	3KDK

*Scattering intensities at low and high scattering angles from the lowest and highest concentrated samples, respectively, were merged using the automerge function from the Primus program in the ATSAS 2.6.0 package.
[&]MW determined using ScÅtter (Rambo and Tainer, 2013).

Supplementary Table 3: List of *Bacillus subtilis* strains

Strain	Characteristics	Source
JRR27	PY79 (SPβ^0)	Simmons et al. 2008 Mol. Cell
PB112	*ΔmutL*	this study
JRR20	*mutL (C69S,C424S,E485C,C531S)*	this study
JRR21	*dnaN (S379,C380) (cat)*	this study
JRR28	*mutL (C69S,C424S,E485C,C531S), dnaN (S379,C380) (cat)*	this study

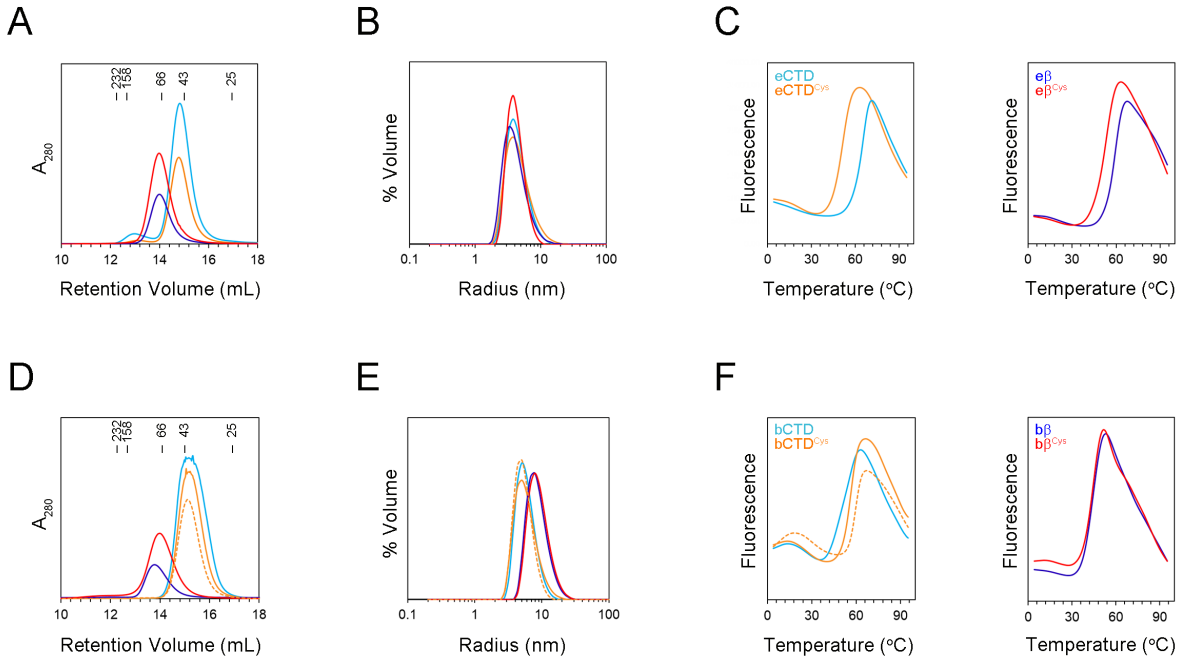

Supplementary Figure 1: Biochemical characterization of the MutL^{CTD} and β proteins. (A) Size exclusion chromatography profiles of *E. coli* MutL^{CTD} and its Cys-variant (light blue and orange), and *E. coli* β and its Cys-variant (dark blue and red). Elution volumes of molecular weight markers (kDa) are indicated. **(B)** Dynamic light scattering particle size distributions of *E. coli* MutL^{CTD}, *E. coli* β and their Cys-variants shown as volume distributions and coloured as in **(A)**. **(C)** Thermal denaturation curves of *E. coli* MutL^{CTD} (left) and β (right) and their Cys-variants measured by differential scanning fluorimetry. **(D)** Size exclusion chromatography profiles of *B. subtilis* MutL^{CTD} (light blue) and its active (solid orange line) and inactive Cys-variants (dash orange line), and *B. subtilis* β and its Cys-variant (dark blue and red). **(E)** Dynamic light scattering particle size distributions of *B. subtilis* MutL^{CTD}, and *B. subtilis* β and their Cys-variants shown as volume distributions and coloured as in **(D)**. **(F)** Thermal denaturation curves of *B. subtilis* MutL^{CTD} (left) and β (right) and their Cys-variants measured by differential scanning fluorimetry.

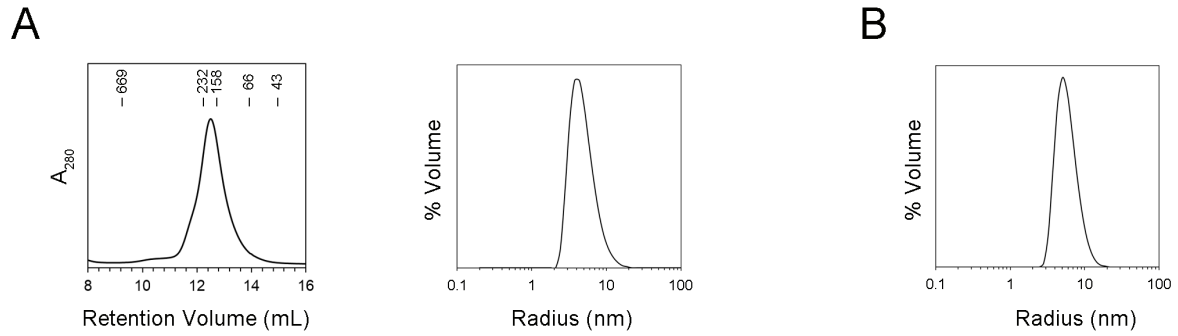

Supplementary Figure 2: Biochemical characterization of the MutL^{CTD}-β complexes. (A) Size exclusion chromatography profiles (left) and dynamic light scattering particle size distributions (right) of the *E. coli* MutL^{CTD}-β complex at 'Day 2'. **(B)** Dynamic light scattering particle size distributions of the *B. subtilis* MutL^{CTD}-β complex.

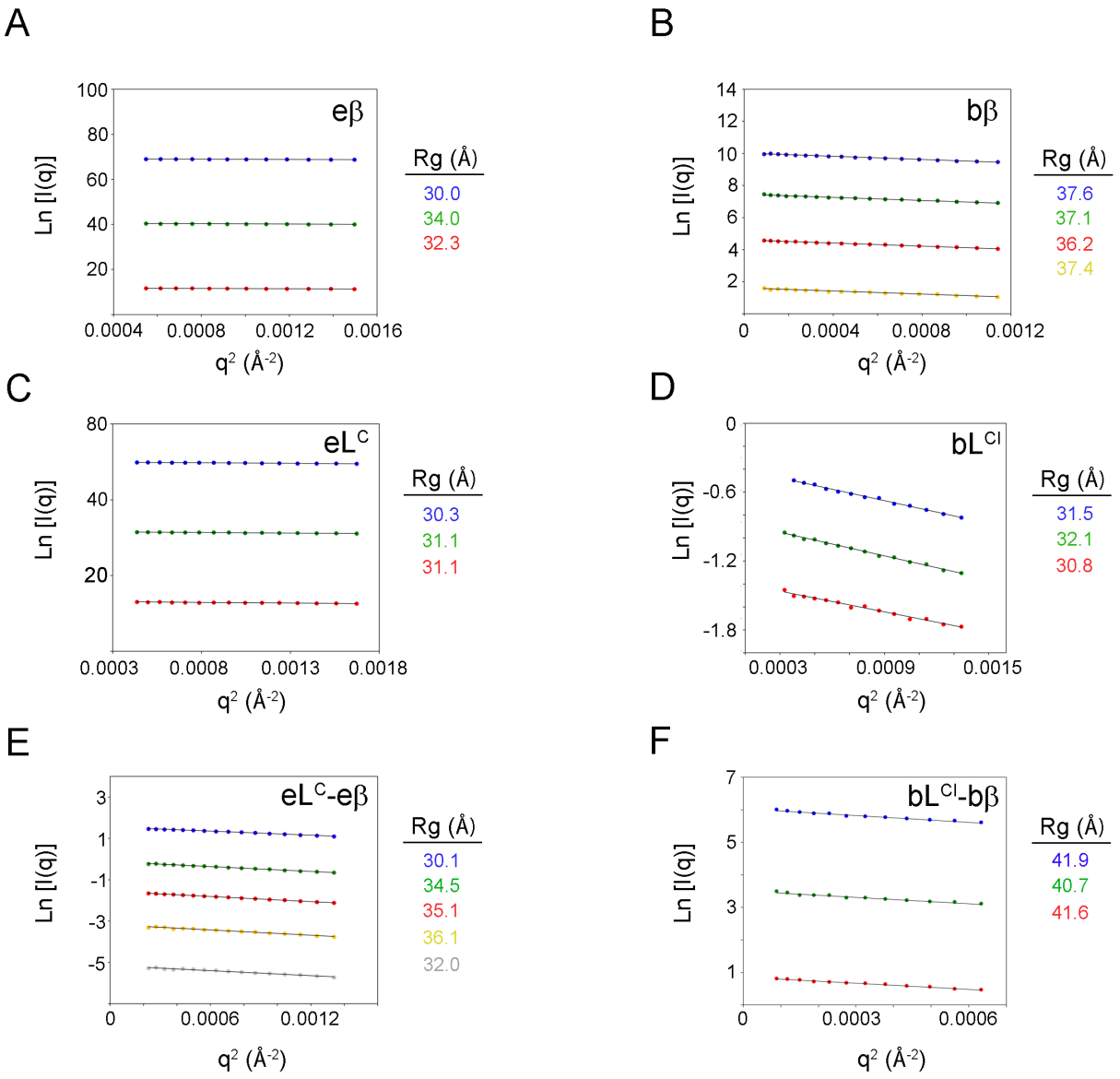

Supplementary Figure 3: Guinier approximation for SAXS scattering curves. Guinier plots for a concentration series (see **Supplementary Table 1**) of eβ **(A)**, bβ **(B)**, eMutL^{CTD} **(C)**, bMutL^{CTDI} **(D)**, eMutL^{CTD}-eβ **(E)** and bMutL^{CTDI}-bβ **(F)** are shown with linear fit (black line). The radius of gyration (Rg) determined in reciprocal space for each concentration is indicated next to each panel. The linearity of the Guinier plots indicates the absence of interparticle interactions.

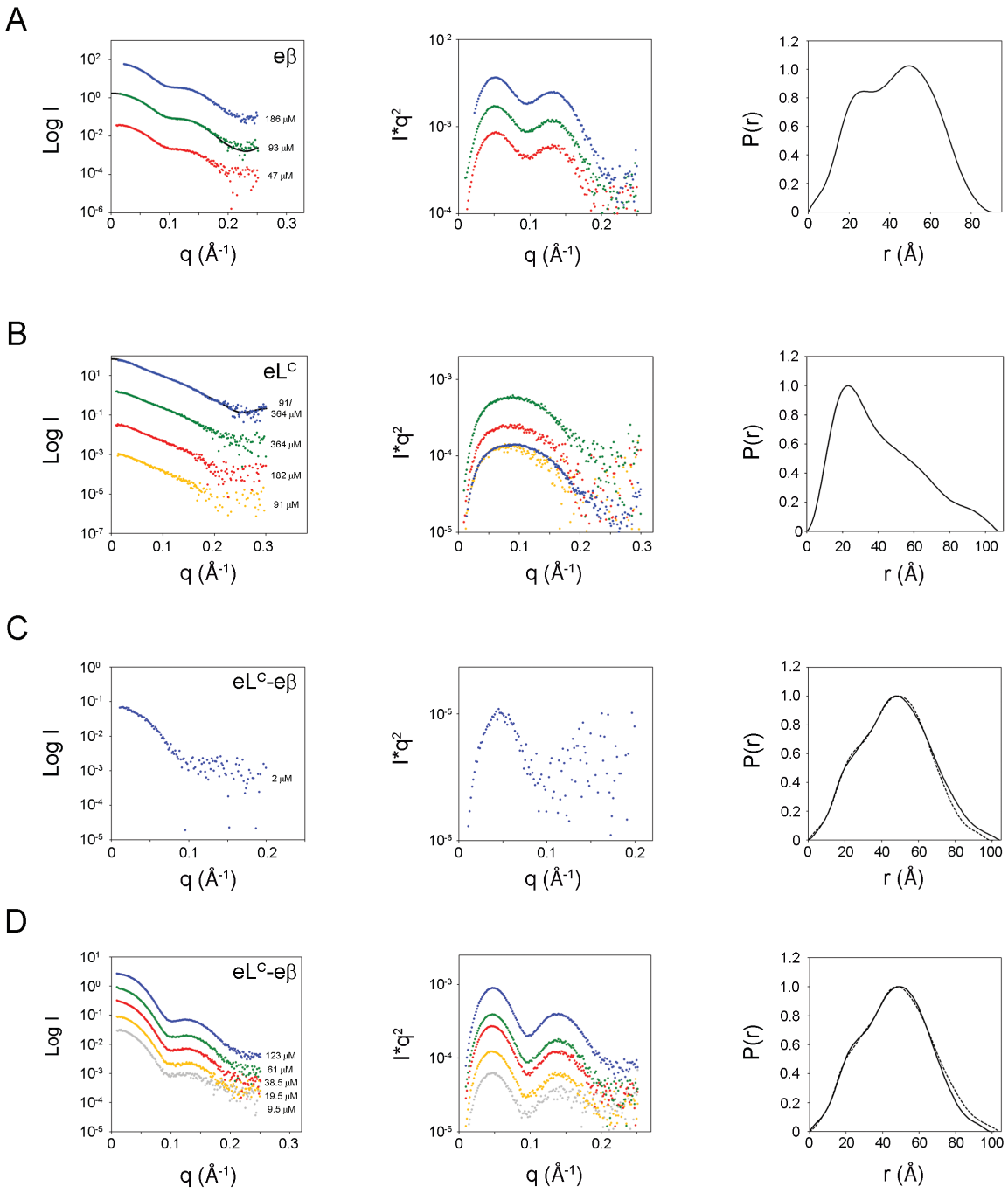

Supplementary Figure 4: SAXS characterization of *E. coli* MutL^{CTD} and β-clamp. Solution scattering (left), Kratky plot (centre) and pair-distance distribution functions (right)) of eβ **(A)**, eMutL^{CTD} **(B)**, eMutL^{CTD}-eβ at 'Day 1' **(C)**, and eMutL^{CTD}-eβ at 'Day2' **(D)**. Theoretical solution scattering calculated with CRYSOL (63) from the atomic structures of β (PDB: 1MMI) and MutL-CTD (PDB: 1X9Z) are shown as solid black lines. The pair-distance distribution functions of 'Day 2' and 'Day 1' are shown as dotted lines in panels **(C)** and **(D)** for comparison.

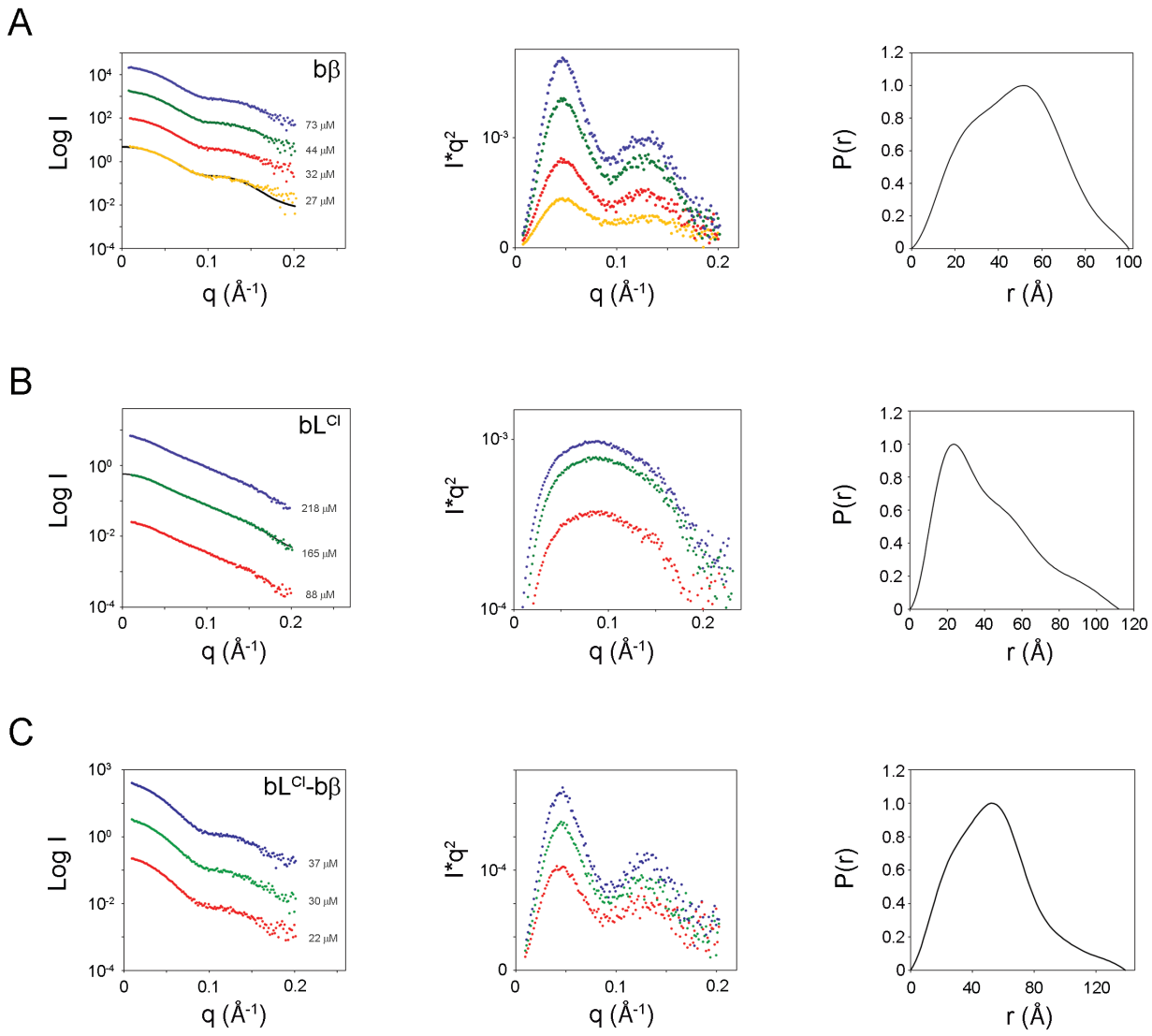

Supplementary Figure 5: SAXS characterization of *B. subtilis* MutL^{CTD} and β-clamp. Solution scattering (left), Kratky plots (center) and pair-distance distribution functions (right) of bβ **(A)**, bMutL^{CTDI} **(B)**, and bMutL^{CTDI}-bβ at 'Day 2' **(C).** Theoretical solution scattering (black line) calculated with CRYSOL (63) from the atomic structures of *B. subtilis* β-clamp (PDB ID 4RT6) and the C-terminal domain of *B. subtilis* MutL (PDB ID 3KDK) are shown as solid black lines with the scattering curves.

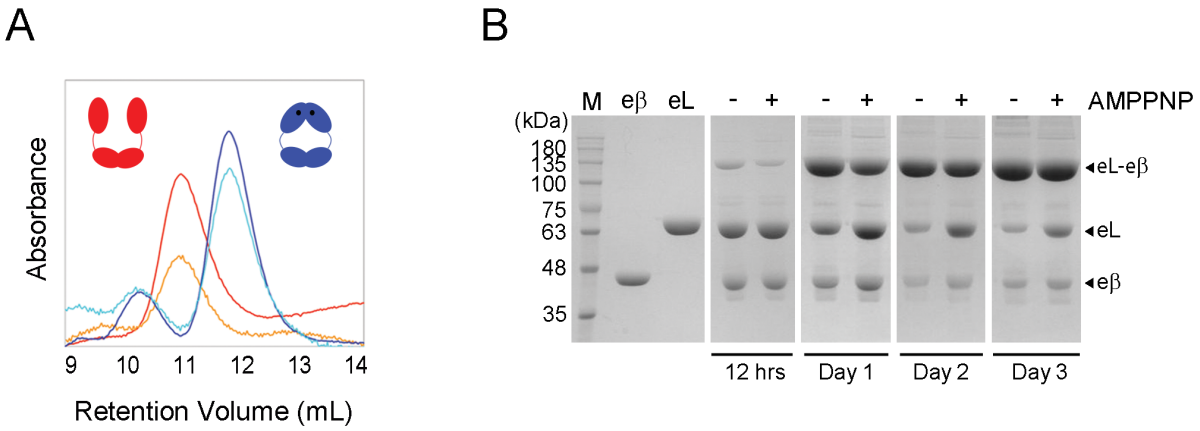

Supplementary Figure 6: *E. coli* MutL interacts with β in a nucleotide-independent manner. (A) Size exclusion chromatography profile of MutL in the absence (red/orange) or presence (blue/cyan) of AMPPNP. The conformational change of MutL and nucleotide binding are monitored by comparing the absorbances at 280 nm (red/blue) and 260 nm (orange/cyan). **(B)** Purified *E. coli* MutL (eL) crosslinked with equimolar amounts of *E. coli* β (eβ) in the presence/absence of AMPPNP resolved on denaturing gels in the absence of β-mercaptoethanol.

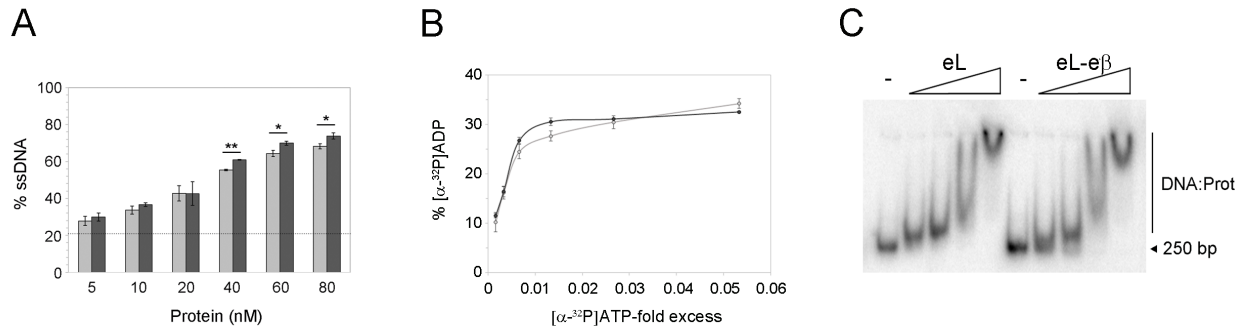

Supplementary Figure 7: The β clamp enhances the MutL-dependent stimulation of UvrD. (A) UvrD helicase activity in the presence of eL (light grey) and eL-eβ (dark grey) on a 250 base-pair nicked DNA. The dotted line denotes the unwinding activity of UvrD in the absence of eL or eL-eβ. Error bars represent the standard deviation of three independent experiments. The p-value was calculated using a two-sample unequal variance t-test. *, $p < 0.013$ and **, $p < 1.4 \times 10^{-4}$. **(B)** ATP hydrolysis activity of eL (grey line) and eL-eβ (black line). Error bars represent the standard deviation of three independent experiments. **(C)** DNA binding of eL and eL-eβ measured using a 250 base-pair DNA.

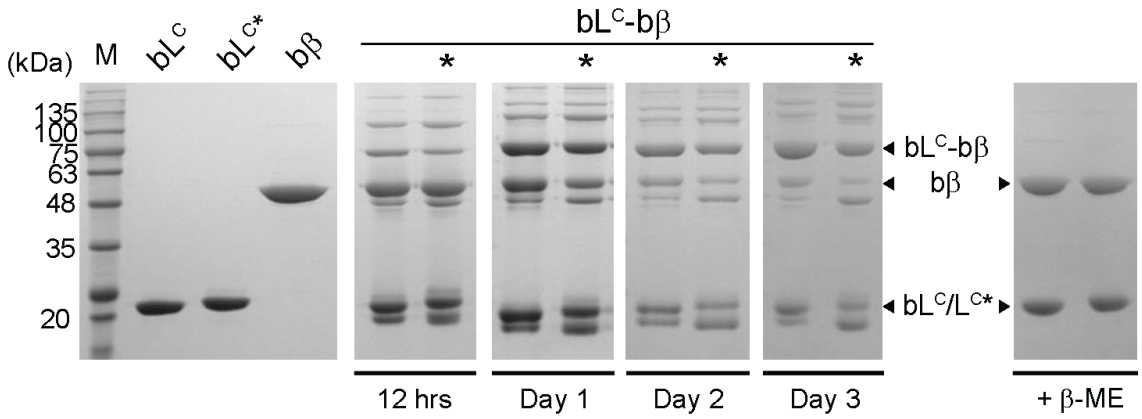

Supplementary Figure 8: Interaction between *B. subtilis* MutL^{CTD} and β. *B. subtilis* β (bβ), the active form of *B. subtilis* MutL^{CTD} (bL^{C}), and a variant of MutL^{CTD} lacking the β-binding motif MutL^{CTD*} (bL^{C*}) were purified and equimolar mixtures of either bL^{C}-bβ or bL^{C*}-bβ were incubated in the absence of reducing agent. Samples withdrawn from the reaction at the indicated time points were resolved on denaturing gels in the absence of β-mercaptoethanol (β-ME).

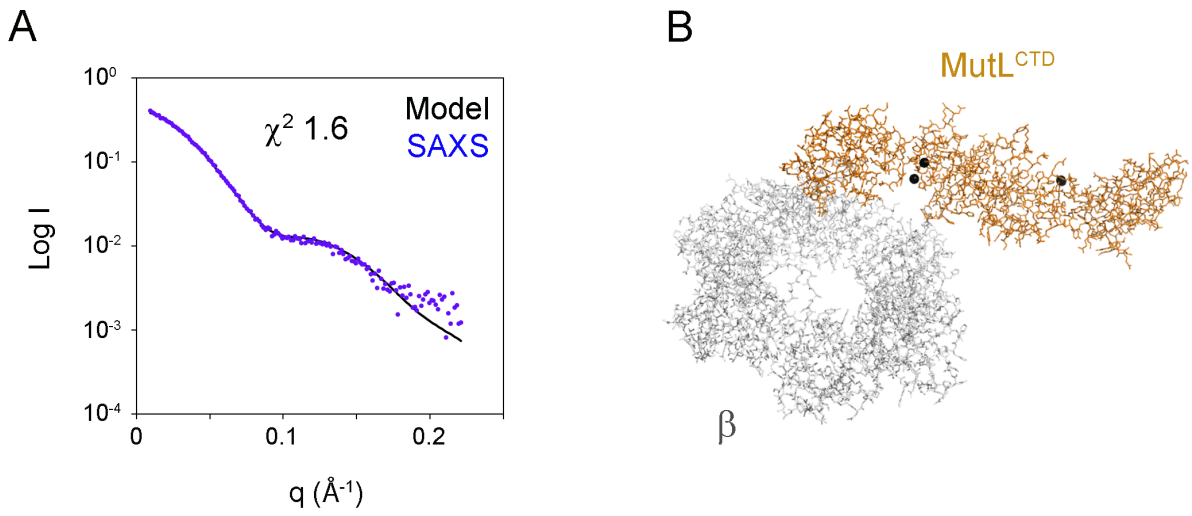

Supplementary Figure 9: Quaternary structure modelling of bMutL^{CTD}-β. (A) SASREF fitting of the *B. subtilis* MutL^{CTD} (PDB 3KDK; orange) is bound at the hydrophobic cleft of β (PDB 4TR6; grey). MutL^{CTD} lies along the edge of the β ring which aligns the proximal MutL endonuclease site with the central cavity of β. Black spheres represent two zinc metals bound at the endonuclease active site of the MutL homodimer.